CONEM
CONGRESSO NACIONAL DE ENGENHARIA MECÂNICA
NATAL - RIO GRANDE DO NORTE - BRASIL

ABCM

XII CONGRESSO NACIONAL DE ENGENHARIA MECÂNICA
DE 29/07 A 02/08 DE 2024, NATAL-RN, BRASIL

CONEM2024-0660
MODELING AND SIMULATION OF A OMNIDIRECTIONAL MULTIROTOR UAV

Fabio Pinheiro Cardoso, fabio.cardoso@cefet-rj.br[1]
João Carlos Virgolino Soares, joao.virgolino@iit.it[2]
Marco Antonio Meggiolaro, meggi@puc-rio.br[3]

[1]C. F. de E. Tecnológica Celso Suckow da Fonseca - CEFET/RJ
[2]Istituto Italiano di Tecnologia - IIT
[3]Pontifícia Universidade Católica do Rio de Janeiro

Abstract: *Multirotor vehicles are broadly used in robotics applications for their low cost, maneuverability, and speed. However, the inability of traditional multirotors to generate thrust and torque independently of each other, and in any direction, has two main consequences. First, the set of viable maneuvers for these Unmanned Aerial Vehicles (UAVs) is severely limited because of the coupling of both position and attitude. Second, the UAVs are unable to withstand arbitrary force and torque disturbances without substantial delay. This is due to the time required to reorient the direction of fixed thrust in the UAV chassis, which degrades the performance of UAVs in scenarios that demand high-precision flight and in scenarios where major external disturbances are found. For instance, in the applications of interaction aerial physics, in activities such as grabbing and manipulating objects or human interaction. This work addresses the modeling and simulations of an omnidirectional multirotor, whose purpose is to overcome the traditional multirotors limitations, i.e., a UAV system capable of independently controlling its thrusts and torques in all degrees of freedom (DOF). The UAV modeling is idealized with eight motors, velocities feedback, and inputs from forces and torques. The typical configurations of conventional multirotor UAVs normally have their motors allocated on the same plane and with their rotation axes parallel to each other. However, the proposal discussed in this work is designed to have its motor-propeller sets configured with eight motors located on the faces of a circumscribed octahedron, and supported by eight beams connected to a core, which can contain all the electronics necessary for its operation. This configuration can enhance the available torque and forces, being able to provide behaviors that are unattainable in common multirotors and has the potential to perform unusual maneuvers for conventional configurations (underactuated) since they can be overactuated or fully actuated depending on the number of installed motor propellers. The analyses, simulations, and preliminary results of the concept of the aerial system are presented, highlighting some requirements, scope, and restrictions.*
Keywords: *omnidirectional, UAV, multirotor, simulation.*

1. INTRODUCTION

Multirotor vehicles are broadly used in robotics applications for their low cost, maneuverability, and speed. However, the inability of traditional multirotors to generate thrust and torque independently of each other, and in any direction, has two main consequences. First, the set of viable maneuvers for these Unmanned Aerial Vehicles (UAVs) is severely limited because of the coupling of both position and attitude, as shown by Jabbari *et al.* (2012), Liu and Yu (2013), Fernandes (2017), Emran and Najjaran (2018) and Schuster *et al.* (2019). Second, the UAVs are unable to withstand arbitrary force and torque disturbances without substantial delay. This is due to the time required to reorient the direction of fixed thrust in the UAV chassis, which degrades the performance of UAVs in scenarios that demand high precision flight and in scenarios where major external disturbances are found. For instance, in the applications of interaction aerial physics, or in activities such as grabbing and manipulating objects or human interaction.

The objective of this work is to analyze an unusual solution for an omnidirectional multirotor with fixed rotors, whose purpose is to overcome the limitations of traditional multirotors, that is, a UAV system capable of independently controlling its thrusts and torques in all degrees of freedom. This configuration has the potential to perform unusual maneuvers for conventional (underactuated) configurations, as they can be overactuated or fully actuated depending on the number of motor-propellers installed.

This work presents the analysis of an omnidirectional multirotor concept, highlighting its requirements, scope and

restrictions. Typical configurations of conventional multirotor UAVs normally have their motors allocated on the same plane and with their rotation axes parallel to each other. However, the proposal discussed in this work has its motor-propeller sets configured with eight motors located on the faces of a circumscribed octahedron, and supported by eight beams connected to a core. This configuration enhances the available torque and forces, being able to provide behaviors that are unattainable in common multirotors.

This work presents a mathematical model for the omnidirectional UAV, whose inputs correspond to the desired forces and torques, and the outputs are the displacements and angles of the aerial platform's attitude, showing through simulations that the behavior of the aerial platform is compatible with an omnidirectional behavior.

2. LITERATURE REVIEW

The common geometry of multirotor aircrafts is a structural arrangement of its propellers in a plane in which the thrust direction is parallel to each other and with vertically directed flow, whose dynamics are non-linear, coupled, multivariable, underactuated or overactuated, subject to uncertainty and with dynamic effects. Omnidirectional UAVs have been developed based on adaptations and combinations of other sustaining principles, contemplating structural and system architecture alterations to provide aerial platforms with omnidirectional capabilities.

Several works have suggested developments of this type, as can be seen in Jeong and Jung (2014), Kim (2017), Elkhatib (2017), and Kamel *et al.* (2018). In these, the concept of a tiltable rotor is widely explored, implying the need to deal with another resulting problem, which is the control allocation matrix. This is because the control allocation matrix in these cases depends on the angle of inclination of the rotor or propeller rotation disk, which makes the treatment of the control problem more complex, as can be seen in Brezak *et al.* (2018), Yao *et al.* (2018), Hamaza and Kovać (2018), Su *et al.* (2019), Xu *et al.* (2020), Allenspach *et al.* (2020), Lu *et al.* (2020), Chen and Jia (2020) and Gao *et al.* (2020). In these works, the general concept of a steerable rotor is explored, using under-actuated or over-actuated platforms, in which, in addition to the steerable rotor, the control allocation problem and control strategies are analyzed. The highlights are Voliro (Elkhatib (2017), Kamel *et al.* (2018), and similar works (by Allenspach *et al.* (2020)), as they provided multirotor platforms with unusual maneuverability in comparison with common platforms.

Brescianini and D'Andrea (2016, 2018) focus their attention on the development of a Multirotor UAV with a three-dimensional configuration, overactuated, with fixed rotors in optimal positions, inscribed in the diagonals of a unitary cube, in order to deliver the maximum thrust available in all directions.

In addition to these, this concept of a solution employing rotors fixed to the frame is also discussed in Hamaza and Kovać (2018), and Dyer (2018), which develops and discusses a platform very similar to the one developed by Brescianini and D'Andrea (2016, 2018).

Also, in Baird *et al.* (2019), Nigro *et al.* (2019), Baird and Nokleby (2020), and Hamandi *et al.* (2021) it is shown solutions involving platforms with fixed rotors in optimized configurations, either fully actuated or overactuated. In these, the problem of allocation and control strategies is not as deeply explored as in the previous ones.

3. METHODOLOGY

To establish the mathematical model, three references are used, according to Fig. 1, namely:
a) the inertial reference or fixed (x0, y0, z0)
b) the body reference, located in the geometric center of the UAV (xb, yb, zb); and
c) the motor reference, located at the motor attachment point.

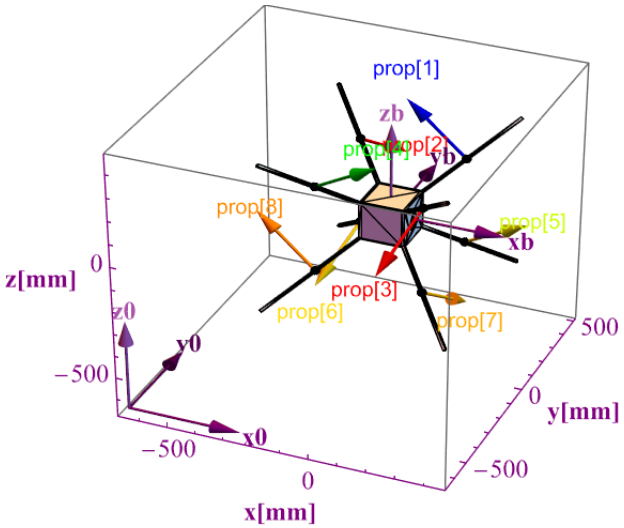

Figure 1: Referencial frame and the motors directions

Considering the concept proposed by Brescianini and D'Andrea (2016, 2018) and Dyer (2018), the mathematical

model can be stated as

$$\begin{bmatrix} \underline{\underline{\boldsymbol{M}}} & \underline{\underline{\boldsymbol{0}}} \\ \underline{\underline{\boldsymbol{0}}} & \underline{\underline{\boldsymbol{J}}} \end{bmatrix} \begin{pmatrix} \underline{\dot{\boldsymbol{v}}} \\ \underline{\dot{\omega}} \end{pmatrix} + \begin{pmatrix} \underline{\omega} \times \underline{\underline{\boldsymbol{M}}} \cdot \underline{\boldsymbol{v}} \\ \underline{\omega} \times \underline{\underline{\boldsymbol{J}}} \cdot \underline{\omega} \end{pmatrix} + \begin{pmatrix} \underline{\underline{\boldsymbol{M}}} \cdot \underline{\boldsymbol{g}} \\ \underline{\underline{\boldsymbol{0}}} \end{pmatrix} = \begin{pmatrix} \underline{\boldsymbol{f}} \\ \underline{\boldsymbol{t}} \end{pmatrix}_{actuating} \tag{1}$$

where $\underline{\underline{\boldsymbol{M}}}$ and $\underline{\underline{\boldsymbol{J}}}$ correspond to the mass and inertia matrices, respectively. The vectors $\underline{\omega}$ and $\underline{\boldsymbol{v}}$ correspond to the angular and linear velocities, respectively. The $\underline{\boldsymbol{g}}$ vector is the gravity acceleration vector. The forces and torque acting on the platform are

$$\begin{pmatrix} \underline{\boldsymbol{f}} \\ \underline{\boldsymbol{t}} \end{pmatrix}_{actuating} = \begin{pmatrix} \underline{\underline{\boldsymbol{X}}} \\ \underline{\underline{\boldsymbol{P}}} \times \underline{\underline{\boldsymbol{X}}} \end{pmatrix} \cdot \underline{\boldsymbol{f}}_{thrust} = \underline{\underline{\boldsymbol{Y}}} \cdot \underline{\boldsymbol{f}}_{thrust} \tag{2}$$

where the thrust model $\underline{f}_{thrust}$ can be defined using either the propeller profile or the motor profile.

The positions and orientations of motors and propellers in the structure are defined by the elements of the $\underline{\underline{\boldsymbol{Y}}}$ matrix, obtained by superposition of two matrices, namely, $\underline{\underline{\boldsymbol{X}}}$, and the term-to-term product of $\underline{\underline{\boldsymbol{P}}}$ and $\underline{\underline{\boldsymbol{X}}}$, as follows.

$$\underline{\underline{\boldsymbol{Y}}} = \begin{pmatrix} \underline{\boldsymbol{X}}_1 & \underline{\boldsymbol{X}}_2 & \underline{\boldsymbol{X}}_3 & \underline{\boldsymbol{X}}_4 & \underline{\boldsymbol{X}}_5 & \underline{\boldsymbol{X}}_6 & \underline{\boldsymbol{X}}_7 & \underline{\boldsymbol{X}}_8 \\ \underline{\boldsymbol{P}}_1 \times \underline{\boldsymbol{X}}_1 & \underline{\boldsymbol{P}}_2 \times \underline{\boldsymbol{X}}_2 & \underline{\boldsymbol{P}}_3 \times \underline{\boldsymbol{X}}_3 & \underline{\boldsymbol{P}}_4 \times \underline{\boldsymbol{X}}_4 & \underline{\boldsymbol{P}}_5 \times \underline{\boldsymbol{X}}_5 & \underline{\boldsymbol{P}}_6 \times \underline{\boldsymbol{X}}_6 & \underline{\boldsymbol{P}}_7 \times \underline{\boldsymbol{X}}_7 & \underline{\boldsymbol{P}}_8 \times \underline{\boldsymbol{X}}_8 \end{pmatrix} \tag{3}$$

Considering that α = 0,788675, β = 0,211325 and γ = 0,57735, the matrices $\underline{\underline{\boldsymbol{P}}}$ and $\underline{\underline{\boldsymbol{X}}}$ correspond to:

a) Position $\underline{\underline{\boldsymbol{P}}}$:

$$\underline{\underline{\boldsymbol{P}}} = \gamma \cdot \begin{bmatrix} 1 & -1 & 1 & -1 & 1 & -1 & 1 & -1 \\ 1 & 1 & -1 & -1 & 1 & 1 & -1 & -1 \\ 1 & 1 & 1 & 1 & -1 & -1 & -1 & -1 \end{bmatrix} \tag{4}$$

b) Orientation $\underline{\underline{\boldsymbol{X}}}$:

$$\underline{\underline{\boldsymbol{X}}} = \begin{bmatrix} -\alpha & \beta & -\beta & \alpha & \alpha & -\beta & \beta & -\alpha \\ \beta & \alpha & -\alpha & -\beta & -\beta & -\alpha & \alpha & \beta \\ \gamma & -\gamma & -\gamma & \gamma & \gamma & -\gamma & -\gamma & \gamma \end{bmatrix} \tag{5}$$

These matrices support the positioning and orientation of the engines, and assist in the design of the aerial platform structure, as well as the platform attitude control system.

Using the Eq. (2), the positioning and orientation of the motors for this case can be verified in Tab. 1, considering that the motor's normal is the propeller rotation axis with the positive direction according to the right-hand rule.

Table 1: Positions and orientations of motors

Propeller motor nº	Position of Normal (x_0, y_0, z_0)	Orientation of Normal (x_f, y_f, z_f)	ang. reference (rad) - (Degree)
1	(0.186667, 0.186667, 0.186667)	(-0.0683247, 0.254991, 0.373333)	2.35619 - 135.
2	(-0.186667, 0.186667, 0.186667)	(-0.118342, 0.441658, 0.)	0.785398 - 45.
3	(0.186667, -0.186667, 0.186667)	(0.118342, -0.441658, 0.)	0.785398 - 45.
4	(-0.186667, -0.186667, 0.186667)	(0.0683247, -0.254991, 0.373333)	2.35619 - 135.
5	(0.186667, 0.186667, -0.186667)	(0.441658, 0.118342, 0.)	0.785398 - 45.
6	(-0.186667, 0.186667, -0.186667)	(-0.254991, -0.0683247, -0.373333)	2.35619 - 135.
7	(0.186667, -0.186667, -0.186667)	(0.254991, 0.0683247, -0.373333)	2.35619 - 135.
8	(-0.186667, -0.186667, -0.186667)	(-0.441658, -0.118342, 0.)	0.785398 - 45.

These positions and orientations are fixed, and this configuration is an optimal arrangement for the thrust maximization, as shown by Brescianini and D'Andrea (2016, 2018), and Dyer (2018). Considering the eight rods arranged according to the diagonals of a cube, Tab. 1 describes the inclinations of the motor's normals with respect to the diagonal planes of the reference cube.

According to Ost (2015), Canal *et al.* (2017) and Gupta and Abdallah (2018), using the propeller profile, considering the motor rotation N, and the propeller diameter D, the thrust behavior T, the power P and the torque Q can be described by Eqs. (6), (7) and (8), as follows:

$$T = C_T \rho N^2 D^4 = f_{thrust} \tag{6}$$

$$P = C_P \rho N^3 D^5 \tag{7}$$

$$Q = C_Q \rho N^2 D^5 = t_{thrust} \tag{8}$$

where C_P is the power coefficient given by the manufacturer, and defined by $C_P = 2\pi C_Q$. C_Q is the torque coefficient, C_T is the thrust coefficient, given by the manufacturer and ρ is the specific-mass in the altitude of flight.

To determine the $\underline{\underline{Y}}$ matrix and its pseudo-inverse $\underline{\underline{Y}}^{\dagger}$, the Eqs. (2)-(5) are used and result in:

$$\underline{\underline{Y}} = \begin{bmatrix} -\alpha & \beta & -\beta & \alpha & \alpha & -\beta & \beta & -\alpha \\ \beta & \alpha & -\alpha & -\beta & -\beta & -\alpha & \alpha & \beta \\ \gamma & -\gamma & -\gamma & \gamma & \gamma & -\gamma & -\gamma & \gamma \\ \beta & -\alpha & \alpha & -\beta & \beta & -\alpha & \alpha & -\beta \\ -\alpha & -\beta & \beta & \alpha & -\alpha & -\beta & \beta & \alpha \\ \gamma & -\gamma & -\gamma & \gamma & -\gamma & \gamma & \gamma & -\gamma \end{bmatrix} \tag{9}$$

$$\underline{\underline{Y}}^{\dagger} = \begin{bmatrix} -\delta & \sigma & \tau & \sigma & -\delta & \tau \\ \sigma & \delta & -\tau & -\delta & -\sigma & -\tau \\ -\sigma & -\delta & -\tau & \delta & \sigma & -\tau \\ \delta & -\sigma & \tau & -\sigma & \delta & \tau \\ \delta & -\sigma & \tau & \sigma & -\delta & -\tau \\ -\sigma & -\delta & -\tau & -\delta & -\sigma & \tau \\ \sigma & \delta & -\tau & \delta & \sigma & \tau \\ -\delta & \sigma & \tau & -\sigma & \delta & -\tau \end{bmatrix} \tag{10}$$

where α = 0,788675, β = 0,211325, γ = 0,57735, $\delta = 0,295753$, $\sigma = 0,0792468$ and $\tau = 0,216506$.

Disregarding the effects of torques produced by the engines and considering that the model for thrusts and torques acting on the platform is the result of the combination of Eqs. (2) and (6), occurs that:

$$\begin{pmatrix} \underline{\boldsymbol{f}} \\ \underline{\boldsymbol{t}} \end{pmatrix}_{6\times 1}^{actuating} = C_T \cdot \rho \cdot D^4 \cdot \underline{\underline{\boldsymbol{Y}}}_{6\times 8} \cdot \underline{\boldsymbol{NSqrd}}_{8\times 1} \tag{11}$$

where $\underline{\boldsymbol{NSqrd}}_{8\times 1}$ is a vector whose elements correspond to the square rotations applied to each motor.

$$\underline{\boldsymbol{NSqrd}}_{8\times 1} = \begin{bmatrix} N_1{}^2 & N_2{}^2 & N_3{}^2 & N_4{}^2 & N_5{}^2 & N_6{}^2 & N_7{}^2 & N_8{}^2 \end{bmatrix}^T \tag{12}$$

Combining the Eq. (12) with the models for thrust produced by the engines in Eq. (6):

$$\underline{\boldsymbol{NSqrd}}_{8\times 1} = (C_T \cdot \rho \cdot D^4)^{-1} \cdot \underline{\underline{\boldsymbol{Y}}}^{\dagger}_{8\times 6} \cdot \begin{pmatrix} \underline{\boldsymbol{f}} \\ \underline{\boldsymbol{t}} \end{pmatrix}_{6\times 1}^{actuating} \tag{13}$$

We use values from APC (2024) to define the propeller parameters, as presented in Tab. 2, where C_P is the power coefficient range, C_T is the the thrust coefficient range, D is the propeller diameter, and p is the propeller pitch. These parameters are defined considering that the propellers are bidirectional, selecting values from three different models. It is possible to estimate the effects and rotations caused by the use of each type of propeller from the parameters summarized in Tab. 2, if applied in Eqs. (11) - (13), which results in rotation estimates for each motor.

Table 2: Parameters of APC Propellers

Propeller	Model 1	Model 2	Model 3
RPM range	1000 - 23000	1000 - 35000	1000 - 24000
C_P range	0,0539 - 0,0427	0,0306 - 0,0284	0,0245 - 0,0297
C_T range	0,0904 - 0,0915	0,0644 - 0,0685	0,0641 - 0,0684
D mm(in) - p mm(in)	127(5) - 101,6(4)	152,4(6) - 76,2(3)	228,6(9) - 114,3 (4,5)

To verify and define some parameters for the tests, the Eq. (13) and the associated parameters from Tabs. 2 are used to get the results of rotations necessary for the aerial platform to overcome gravity and remain in hover in simulation, considering a UAV with a mass of $m_{total} = 3,0$ kg.

As we wish to integrate this modeling for the thrusts with the modeling of the dynamic behavior of the UAV, the Eq. (1) is revisited. By explaining the vector of accelerations and variations in angular speeds, it is possible to estimate speeds, displacements and attitude over time, and thus simulate dynamic behavior as

$$\begin{pmatrix} \dot{\underline{\boldsymbol{v}}} \\ \dot{\underline{\omega}} \end{pmatrix} = \begin{pmatrix} \underline{\underline{\boldsymbol{M}}}^{-1} \cdot \underline{\boldsymbol{f}}^{actuating} \\ \underline{\underline{\boldsymbol{J}}}^{-1} \cdot \underline{\boldsymbol{t}}^{actuating} \end{pmatrix} - \begin{pmatrix} \underline{\underline{\boldsymbol{M}}}^{-1} \cdot \underline{\omega} \times \underline{\underline{\boldsymbol{M}}} \cdot \underline{\boldsymbol{v}} \\ \underline{\underline{\boldsymbol{J}}}^{-1} \cdot \underline{\omega} \times \underline{\underline{\boldsymbol{J}}} \cdot \underline{\omega} \end{pmatrix} - \begin{pmatrix} \underline{\boldsymbol{g}} \\ \underline{\boldsymbol{0}} \end{pmatrix} \tag{14}$$

In this work, the Eq. (14) is solved using numerical integration using the 4th order Runge-Kutta method. The equations are solved in stages since a controller is not considered and the system's response is non-linear and occurs based on the constraints of the problem. To monitor the evolution of the system's response, this simulation is carried out at intervals of 1.0 second based on the forces and torques applied in the local reference of the UAV body and the final conditions of the previous states, with the exception of the first, where the conditions initials are null or prescribed altitude.

4. RESULTS

The input forces and torques can be viewed in Tab. 3, and combined with the initial conditions, generate the presented results. The inputs considered for the solutions corresponded to:

Table 3: The input forces and input torques for simulation

Simulation Range	$f_x[N]$	$f_z[N]$	$t_x[N.m]$
from t = 0 to t = 1	0	35,0	0
from t = 1 to t = 2	5,0	32,5	0
from t = 2 to t = 3	-5,0	29,5	0
from t = 3 to t = 4	0	29,5	5,0
from t = 4 to t = 5	0	34,0	-2,5

where $f_y = t_y = t_y = 0$.

The simulation results represent the displacements, attitude and their rates of change over time, arranged in 1.0 second intervals, whose results are concatenated, i.e., the final result of each interval is the initial condition of the following interval. These results are presented in Figs. 2, 4, 6, 8 and 10.

As discussed in the methodology, the engine thrust directions for some operating modes are summarized in Tab. 4, constructed using Eq. (11), taking as a starting point the initial directions described in Tab. 1, and corresponding to the operating modes for the engines used in the dynamics simulation. These thrust components for each engine can be seen in Figs. 3, 5, 7, 9 and 11.

Table 4: Directions of thrusts for some mode of operations

Propeller	Lifting in $+z_0$	Translation in $+x_0$	Translation in $-x_0$	Rotation in $+x_0$	Rotation in $-x_0$
[1]	1	-1	1	1	1
[2]	-1	-1	-1	-1	1
[3]	-1	-1	-1	1	-1
[4]	1	1	-1	1	1
[5]	1	1	-1	1	1
[6]	-1	-1	-1	-1	1
[7]	-1	-1	-1	1	-1
[8]	1	-1	1	1	1

In Fig. 2 it is shown the behavior of the UAV, considering that it was at rest at t = 0 and at an altitude of 0.25 m, reaching about 1,2 m altitude after taking off. In Fig. 3, the rotation directions of the rotor normals in the take-off condition are shown. Figure 4 shows the UAV evolution from the final state of the previous interval, namely, $p_x(1)$, $p_y(1)$, $\phi(1)$, $\theta(1)$, ψ, $u(1)$, $p(1)$, $q(1)$ and $r(1)$ equal to zero. The $p_z(1)$ is $1,18m$ and $w(1)$ is equal to $1,86m/s$. In this interval, in addition to the force for climbing being reduced to around $32,362N$, a force of $5,0N$ was also applied in the x direction to make a displacement in this x axis, as can be seen in the Fig. 4. In Fig. 5, the rotation directions of the rotor normals under ascent and translation conditions are shown.

In the interval $t = 2,0s$ and $t = 3,0s$, some initial conditions are modified, retaining only the variables $p_y(2)$, $\phi(2)$, $\theta(2)$, ψ, $p(2)$, $q(2)$ and $r(2)$ equal to zero. The variables that were modified are $p_x(2) = 0,833m$, $u(2) = 1,66m/s$ and $w(2) = 2,841m/s$. In this stage, the minimum force to sustain the flight is maintained and a counter force of $-5,0N$ in the x direction is applied in order to brake the horizontal displacement of the UAV, as shown in Fig. 6. In Fig. 7, the rotation directions of the rotor normals under ascent and x bracking conditions are shown. Under these conditions, it is possible to perceive the independence of the altitude and horizontal displacement evolution without interfering with the other degrees of freedom (translations and rotations).

To evaluate the behavior in rotation, the rotational movement around the x axis was simulated, starting from the initial conditions $p_y(3)$, $\phi(3)$, $\theta(3)$, ψ, $u(3)$, $v(3)$, $p(3)$, $q(3)$ and $r(3)$ equal to zero and $p_x(3) = 0,833m$, $p_z(3) = 6,371m$, $w(3) = 2,841m/s$. Under these conditions, a torque of 5,0 N.m around the x axis was applied and the flight lift force $f_z(3)$ was maintained at around $29,4N$. The results can be seen in Fig. 8. In Fig. 9, the rotation directions of the rotor normals under ascent and $+x$ rotations conditions are shown.

At this stage, it is possible to verify that there are no significant interferences in the translational degrees of freedom (p_x, p_y e p_z), in addition to also observing that the rotational degrees of freedom (θ e ψ) not affected by the action of torque have also not suffered disturbances from possible couplings, as shown in Fig. 8.

In the fifth and final stage of the simulation, the initial conditions $\theta(4)$, $\psi(4)$, $u(4)$, $q(4)$ and $r(4)$ are equal to zero and $p_x(4) = 0,833m$, $p_x(4) = 1,66m$, $p_y(4) = -1,045m$, $p_z(4) = 8,02m$, $\phi(4) = 3,125rad$, $v(4) = 3,25m/s$, $w(4) = -1,566m/s$ and , $p(4) = 6,25rad/s$. A counter torque t_x of $-2,5N.m$ is applied and the flight maintenance

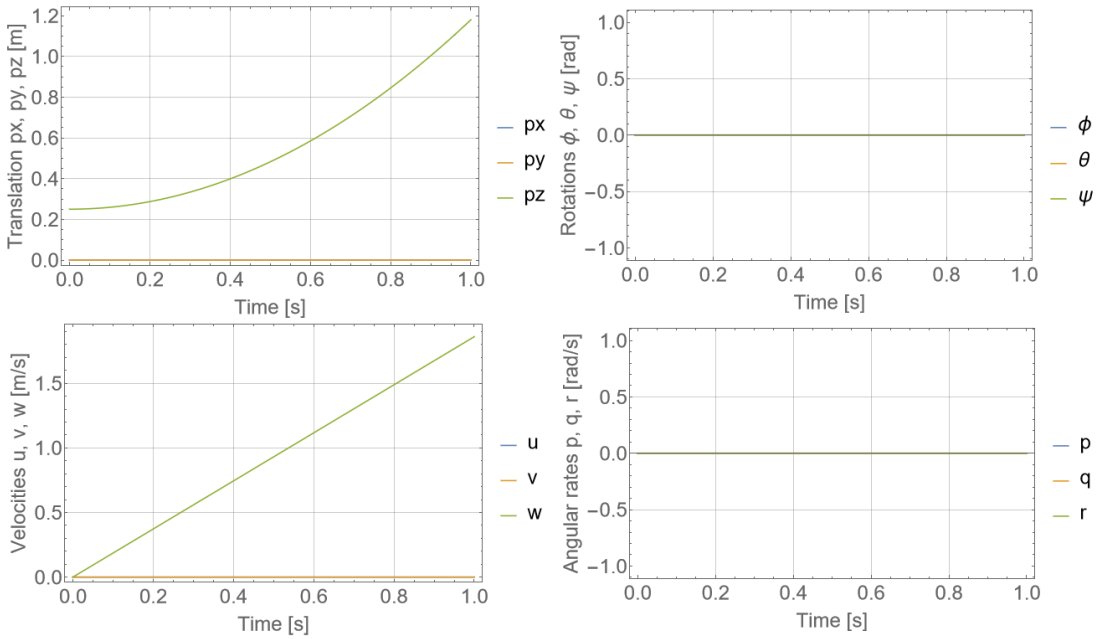

Figure 2: Dynamical behaviour in t = [0,1] seconds.

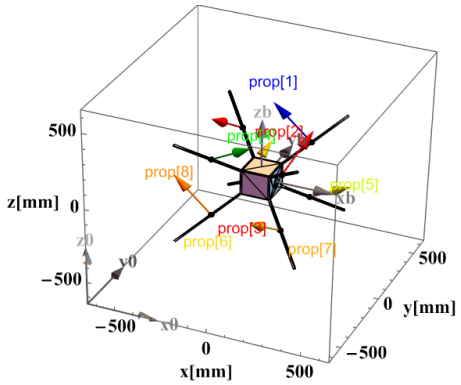

Figure 3: Thrusts directions for motors in take-off and lifting movement z.

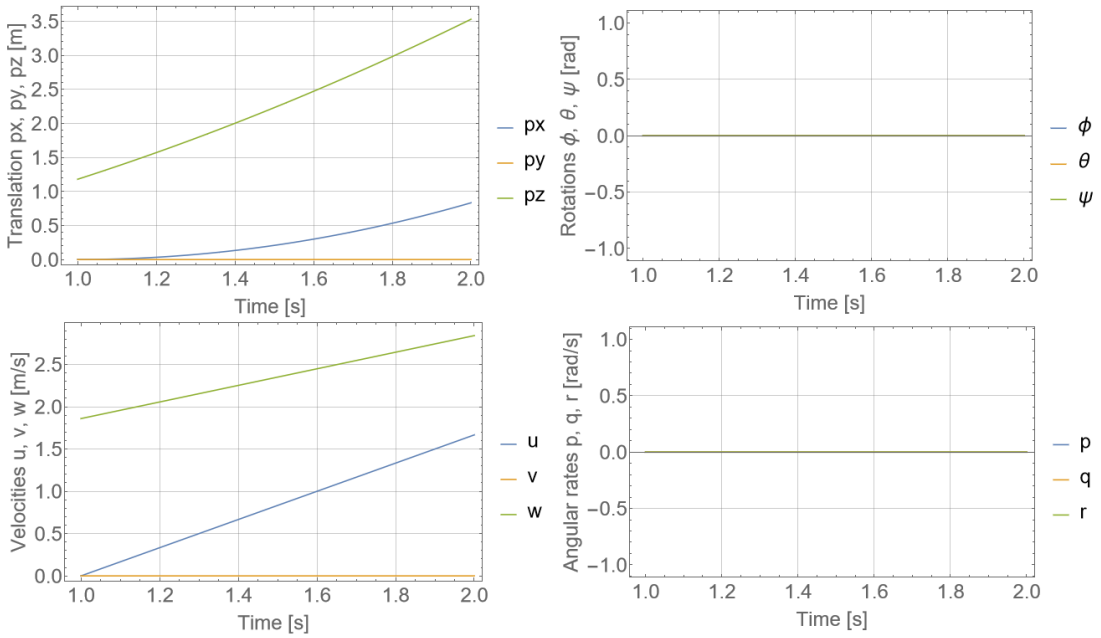

Figure 4: Dynamical behaviour in t = [1,2] seconds.

force f_z is increased to $33,85N$, as shown in Fig. 10. At the end of this fifth stage, the UAV's position is $p_x = 1,8m$, $p_y = -1,8m$ and $p_z = 7,8m$ and attitude with $\phi = 7.8rad$, $\theta = \psi = 0$. In Fig. 11 the rotation directions of the rotor normals under ascent and $-x$ rotations conditions are shown.

An interesting aspect of the results has to do with the characteristics of omnidirectionality, i.e., the ability to act on

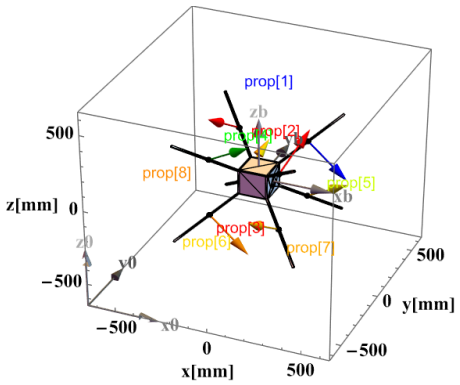

Figure 5: Thrusts directions in lifting and translation in the x axis$(+)$.

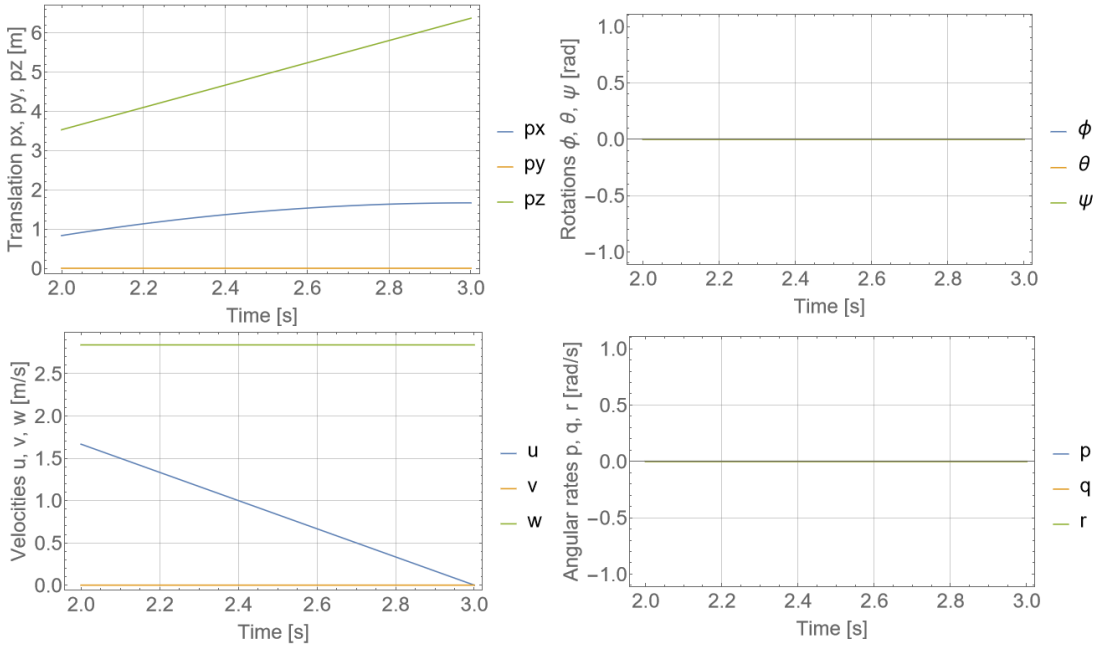

Figure 6: Dynamical behaviour in t = [2,3] seconds.

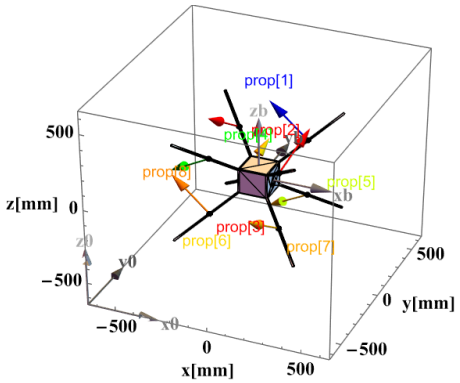

Figure 7: Thrusts directions in lifting and rotation in the x axis$(+)$.

all six degrees of freedom independently. A common multirotor needs to combine two actuations to obtain horizontal movements, given its underactuation characteristic. In the results presented, it is possible to perceive the action occurring only in the acted degrees of freedom, without any signs of action in the others, corroborating some characteristics of omnidirectionality.

5. CONCLUSION

This work presented the mathematical modeling and the simulations of an omnidirectional UAV with fixed motors, addressing some requirements and restrictions. Also, it was presented initial simulations of hovering flight and moving. Future works will include the analysis of motors-propellers arrangement, the structural studies of a rigid nucleus, the development of a chassis with a structural core rigid enough to dispense with protective edges and studies of the control subsystem. The results presented emphasize the promising aspect of this concept, particularly in its omnidirectional

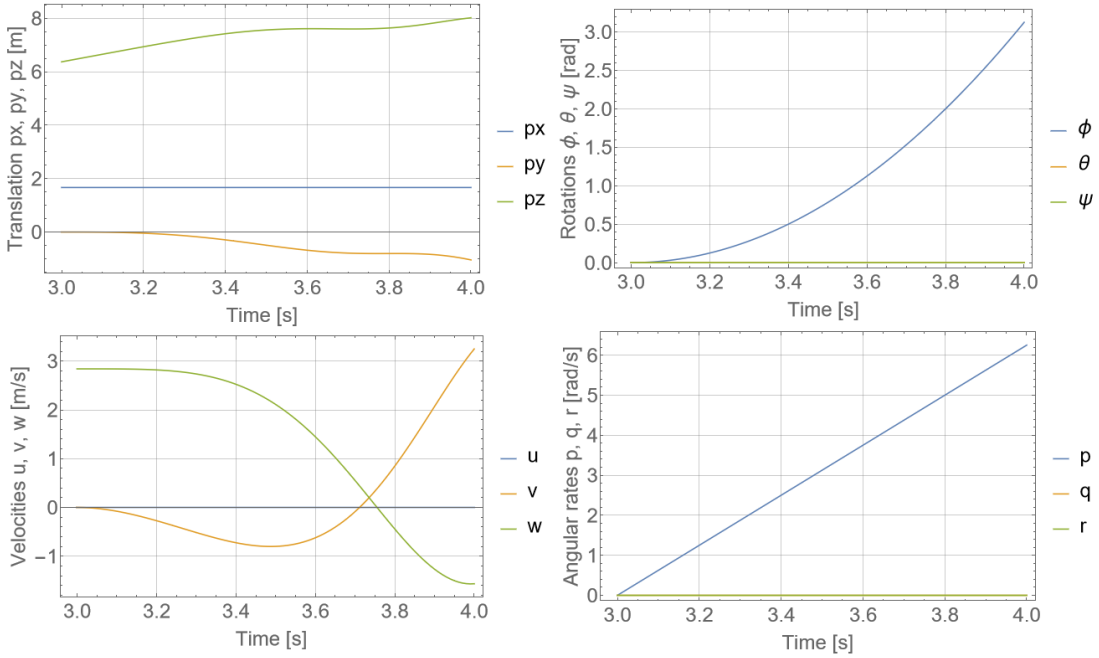

Figure 8: Dynamical behaviour in t = [3,4] seconds.

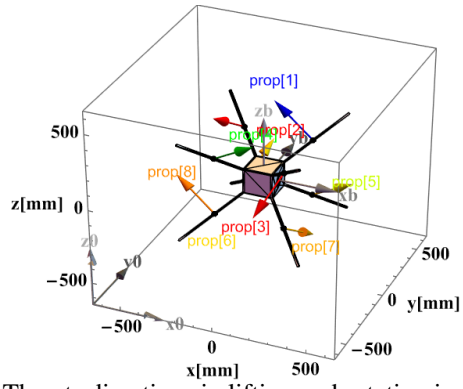

Figure 9: Thrusts directions in lifting and rotation in x axis$(-)$.

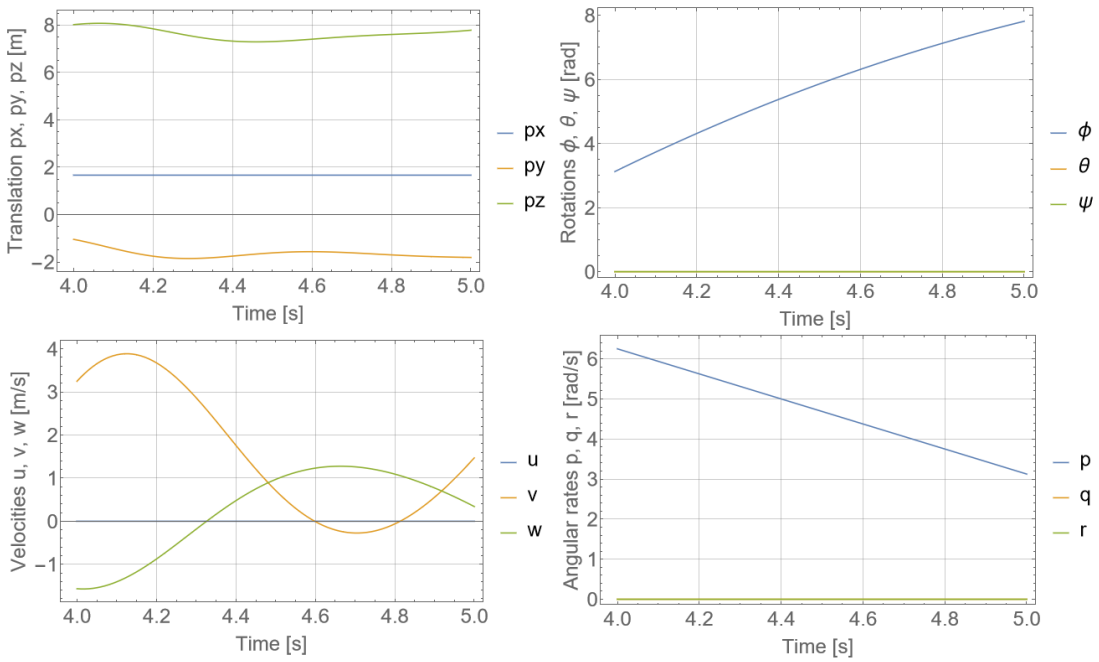

Figure 10: Dynamical behaviour in t = [4,5] seconds.

characteristics, and encourage future studies to be carried out.

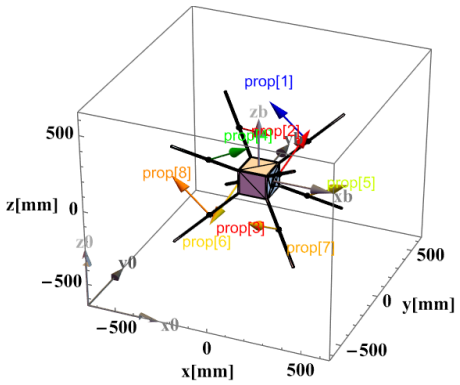

Figure 11: Thrusts directions in lifting and rotation in the x axis$(-)$.

6. REFERENCES

Allenspach, M., Bodie, K., Brunner, M., Rinsoz, L., Taylor, Z., Kamel, M., Siegwart, R. and Nieto, J., 2020. "Design and optimal control of a tiltrotor micro-aerial vehicle for efficient omnidirectional flight. the international journal of robotics research". *The International Journal of Robotics Research - SAGE*. doi:10.1177/0278364920943654.

APC, 2024. "APC Propeller". `https://www.apcprop.com/technical-information/performance-data/`. [Online; accessed 12-June-2024].

Baird, C., Frankenberg, F.V. and Nokleby, S.B., 2019. "Design and development of a next generation omni-directional multirotor". In *Canadian Committee for the Theory of Machines and Mechanisms, Mechanisms, Machines, and Mechatronics (M3) Symposium (CCToMM)*. URL `http://www.cctomm.ca/2019/P15.pdf`.

Baird, C. and Nokleby, S., 2020. "Autonomous Perching of an Omni-Directional Unmanned Aerial Vehicle". In *11th IEEE Annual Information Technology, Electronics and Mobile Communication Conference (IEMCON)*. pp. 0553–0558. doi:10.1109/IEMCON51383.2020.9284825.

Brescianini, D. and D'Andrea, R., 2016. "Design, modeling and control of an omni-directional aerial vehicle". In *2016 IEEE International Conference on Robotics and Automation (ICRA)*. pp. 3261–3266. doi:10.1109/ICRA.2016.7487497.

Brescianini, D. and D'Andrea, R., 2018. "An omni-directional multirotor vehicle". *Mechatronics*, Vol. 55, pp. 76–93. ISSN 0957-4158. doi:10.1016/j.mechatronics.2018.08.005. URL `https://www.sciencedirect.com/science/article/pii/S0957415818301314`.

Brezak, H., Kasać, J., Kotarki, D. and Piljek, P., 2018. "Chattering-free tracking control of a fully actuated multirotor with passively tilted rotors". *Transations of FAMENA*, Vol. 42, No. 1. doi:10.21278/TOF.42101.

Canal, I.P., Reimbol, M.P. and Luft, C., 2017. "Motor brushless: Modelagem matemática e sua dinâmica". In *Proceeding Series of the Brazilian Society of Computational and Applied Mathematics*. Vol. 5. doi:10.5540/03.2017.005.01.0177.

Chen, Z. and Jia, H., 2020. "Design of Flight Control System for a Novel Tilt-Rotor UAV". *Complexity*. ISSN 0921-8890. doi:10.1155/2020/4757381.

Dyer, E., 2018. *Modelling and Control of an Omni-directional UAV*. Dissertação (Mestrado em Ciências Aplicada), McMaster University, Hamilton - Canada.

Elkhatib, O., 2017. *Control Allocation of a Tilting Rotor Hexacopter*. Trabalho de conclusão de curso, ETH Zurich, Zurich. doi:10.3929/ethz-b-000224598.

Emran, B.J. and Najjaran, H., 2018. "A review of quadrotor: An underactuated mechanical system". *Annual Reviews in Control*, Vol. 46, pp. 165–180. doi:10.1016/j.arcontrol.2018.10.009. URL `https://www.sciencedirect.com/science/article/pii/S1367578818300932`.

Fernandes, J.M.M., 2017. *Controle inteligente de sistemas subatuados com aplicações em problemas de mecânica do contato*. Ph.D. thesis, Universidade Federal do Rio Grande do Norte - UFRN.

Gao, J., Zhang, Q. and Chen, J., 2020. "EKF-Based Actuator Fault Detection and Diagnosis Method for Tilt-Rotor Unmanned Aerial Vehicles". *Mathematical Problems in Engineering*. doi:10.1155/2020/8019017.

Gupta, G. and Abdallah, S., 2018. "Propeller force-constant modeling for multirotor uavs from experimental estimation of inflow velocity". *International Journal of Aerospace Engineering*, Vol. 2018, p. 10. doi:10.1155/2018/9632942.

Hamandi, M., Usai, F., Sablé, Q., Staub, N., Tognon, M. and Franchi, A., 2021. "Design of Multirotor Aerial Vehicles: A Taxonomy Based on Input Allocation". *The International Journal of Robotics Research*. doi:10.1177/02783649211025998.

Hamaza, S. and Kovać, M., 2018. "Omni-Drone: on the Design of a Novel Aerial Manipulator with Omni-directional Workspace". pp. 153–158. doi:10.1109/UR49135.2020.9144837.

Jabbari, H., Oriolo, G. and Bolandi, H., 2012. "Dynamic ibvs control of an underactuated uav". In *2012 IEEE International Conference on Robotics and Biomimetics (ROBIO)*. pp. 1158–1163. doi:10.1109/ROBIO.2012.6491126.

Jeong, S.H. and Jung, S., 2014. "A quad-rotor system for driving and flying missions by tilting mechanism of rotors from design to control". *Mechatronics*, Vol. 24, pp. 1178 – 1188. doi:10.1016/j.mechatronics.2014.09.006.

Kamel, M., Verling, S., Elkhatib, O., Sprecher, C., Wulkop, P., Taylor, Z., Siegwart, R. and Gilitschenski, I., 2018. "The voliro omniorientational hexacopter: An agile and maneuverable tiltable-rotor aerial vehicle". *IEEE Robotics and Automation Magazine*, Vol. 25, No. 4, pp. 34–44. doi:10.1109/mra.2018.2866758.

Kim, J., 2017. *Design & Control of An Omni-directional Quadrotor*. Dissertação (Mestrado em Ciências), Texas A M University, Texas - USA.

Liu, Y. and Yu, H., 2013. "A survey of underactuated mechanical systems". *IET Control Theory & Applications*, Vol. 7, pp. 921–935. doi:10.1049/iet-cta.2012.0505. URL `https://ietresearch.onlinelibrary.wiley.com/doi/abs/10.1049/iet-cta.2012.0505`.

Lu, K., Yang, Z., Liao, L., Jiang, Y., Xu, C., Xu, H. and Zhang, Q., 2020. "Extended state observer-based robust control of an omnidirecional quadrotor with tiltable rotors". *Transactions of the Institute of Measurement and Control - SAGE*, Vol. 43, No. 5. doi:10.1177/0142331220966427.

Nigro, M., Pierri, F. and Caccavale, F., 2019. "Preliminary design, modeling and control of a fully actuated quadrotor uav". In *2019 International Conference on Unmanned Aircraft Systems (ICUAS)*. pp. 1108–1116. doi:10.1109/ICUAS.2019.8798092.

Ost, A., 2015. *Modelagem Matemática do Conjunto ESC-Motor-Hélice de um VANT Utilizando Identificação de Sistemas*. Dissertação de mestrado em modelagem matemática, Universidade Regional do Noroeste do Estado do Rio Grande do Sul - UNIJUÍ.

Schuster, M., Bernstein, D., Yao, C., Jansheck, K. and Beitelschmidt, M., 2019. "Comparison of design approaches of fully actuated aerial robots based on maximum wrench generation and minimum energy consumption". *International Federation of Automatic Control (IFAC) 2019*, Vol. 52, pp. 603–608. doi:10.1016/j.ifacol.2019.11.742.

Su, J., Su, C., Xu, S. and Yang, X., 2019. "A Multibody Model of Tilt-Rotor Aircraft Based on Kane's Method". *International Journal of Aerospace Engineering - Hindawi*. doi:10.1155/2019/9396352.

Xu, H., ang K Lu, Z.Y., Xu, C. and Zhang, Q., 2020. "Control of a Tilting Hexacopter under Wind Disturbance". *Mathematical Problems in Engineering - Hindawi*. doi:10.1155/2020/9465153.

Yao, C., Krieglstein, J. and Janschek, K., 2018. "Modeling and Sliding Mode Control of a Fully-actuated Multirotor with Tilted Propellers". In *2018 International Federation of Automatic Control (IFAC)*. Vol. 51, pp. 115–120. doi:10.1016/j.ifacol.2018.11.527.

7. RESPONSIBILITY NOTICE

The author(s) is (are) solely responsible for the printed material included in this paper.